Monte Carlo Simulation of Siemens Primus plus Linac for 6 and 18 MV Photon Beams

Dowlatabadi H.[1], Mowlavi A. A.[2,3]*, Ghorbani M.[4], Mohammadi S.[1]

[1]Physics Department, School of Sciences, Payame Noor University of Mashhad, Mashhad, Iran
[2]Physics Department, School of Sciences, Hakim Sabzevari University, Sabzevar, Iran
[3]ICTP, Associate Federation Scheme, Medical Physics Field, Trieste, Italy
[4]Biomedical Engineering and Medical Physics Department, Faculty of Medicine, Shahid Beheshti University of Medical Sciences, Tehran, Iran

ABSTRACT

Objective: The aim of the present study is to simulate 6 MV and 18 MV photon beam energies of a Siemens Primus Plus medical linear accelerator (Linac) and to verify the simulation by comparing the results with the measured data.

Methods: The main components of the head of Siemens Primus Plus linac were simulated using MCNPX Monte Carlo (MC) code. To verify the results, experimental data of percentage depth dose (PDD) and beam dose profile for 5 × 5 cm^2, 10 × 10 cm^2 and 20 × 20 cm^2 field sizes were measured and compared with simulation results. Moreover, gamma function was used to compare the measurement and simulation data.

Results: The results show a good agreement, within 1%, was observed between the data calculated by the simulations and those obtained by measurement for 6 MV photon beam, while it was within 2% for 18 MV photon beam, except in the build-up region for both beams. Gamma index values were less than unity in most data points for all the mentioned energies and fields. To calculate the dose in the phantom, cells were selected in different modes, one of the modes due to the lack of dose gradient and overlapping, produced better results than others produce.

Conclusion: There was good settlement between measured and MC simulation values in this research. The simulation programs can be used for photon modes of Siemens Primus Plus linac in conditions in which it is not possible to perform experimental measurements.

Keywords

Radiotherapy, Siemens Primus plus Linac, MC Simulation, 6 and 18 MV Photon Beams, Gamma Function

Introduction

Cancer patients can be treated by radiation alone or by combined methods with surgery or treatment by chemicals, immunological and genetic treatment [1]. Radiation remedy is a stable procedure of cancer remedy. Several kinds of radiotherapy are determinate today, diverse in the kinds of radiation delivery. One method of irradiation uses a linac [2]. Monte Carlo method is an actuarial simulation technique. Monte Carlo technique can model the physical processes involved in radiation therapy and is strong in behavior with any complex geometry [3-4].

Many studies have been executed in photon fields with various linacs by various codes such as Monte Carlo N-Particle transport code

*Corresponding author:
A. A. Mowlavi
Physics Department, School of Sciences, Hakim Sabzevari University, Tohid Shahr, Sabzevar, Iran
E-mail: amowlavi@hsu.ac.ir

Received: 5 April 2017
Accepted: 30 April 2017

(MCNP), electron gamma shower (EGS4), GEANT4 and penetration and energy loss of positrons and electrons (PENELOPE). For example, recently Al Jamal and Zakaria obtained dose distribution produced by 6 MV photon beam of Siemens Primus linear accelerator through simulating this linac [5]. The difference between simulation and measurement results was 2%.

Grevillot et al. used GEANT4 method to simulate 6 MV photon beam of an Elekta linac [6]. Sardari et al. computed depth dose of Siemens primus linac using Geant4 [7]. There was good settlement between the measured and the MC simulations data for 6 MV photons, and there is a minimum statistical discrepancy between the data. Siemens Primus linac was modeled in its 15 MV mode with MCNPX code in the thesis of Becker [8]. Additionally, major components of head of 15 MV photon beam of Siemens linac were simulated in the thesis of Mohammadi and the results were published. This calculation is performed using MCNPX Monte Carlo code [9].

Although many studies have been carried out in different photon fields with different linacs, a few studies have used Siemens Primus Plus accelerator at higher energies (18 MV). For this reason, this accelerator was selected in this study. The aim of the present study is to simulate 6 MV and 18 MV photon beam energies of a Siemens Primus Plus linac and to verify the simulation by comparing the results with the measured data.

Material and Methods

In this study, a Siemens Primus Plus medical linac was simulated by MCNPX code. This machine has two treatment modes: photon and electron. The photon mode in this machine has two nominal energies: 6 and 18 MV, and works with six nominal electron energies: 6, 8, 10, 12, 15 and 18 MeV. Matching the task group report No. 105 (TG-105) reportage by the American community of Physicists in Medical profession, measurement should be done under the same situation as the MC simulation [14]. The linac head geometry was modelled using MCNPX 2.7.0 MC code. Water phantom was defined as a cube with dimensions of 50 cm × 50 cm × 50 cm, the surface of which was 100 cm far from the source [11].

The electron source was considered as a 2 mm radius tablet, producing electrons with a Gaussian energy distribution. The optimized energy of the electron spectrum was selected within ± 0.2 MeV energy range self-relative to the manufacturer-provided energy spectrum. The selection of the optimized energy was firmly fixed on the settlement of build-up depth specified from MC simulations with empirical measurement [9].

The target is of cylindrical scheme with a height of about 1.5 cm and a diameter of approximately 3 cm. The simulated geometry of the linac head is shown in Figure 1. The modelling included target, absorber, primary collimator (PC), photon dose chamber, flattening filter (FF) and jaws. The material components of the linac head are given in Table 1.

In this accelerator, the flattening filter which is made of stainless steel, is more complex for 18 MV photon beam, and different from that which is used for 6 MV photon beam as listed in Tables 2 and 3. The mirror is aligned along the gun-target axis and the top of the mirror is tilted towards the target. The primary collimator is made of tungsten and is located directly under the target having a height of about 6.52 cm and an extrinsic diameter of about 7.5 cm. The absorber is made of Aluminium and is positioned inside the primary collimator closely under the target. It is 1.27 cm high and has a maximum diameter of slightly less than 2 cm.

In the present study, MC simulations were run using a personal computer with Intel(R) processor of core i7™, with 4.00 GHz speed, and a 64-bit operating system. The energy cut-off and the cell importance were selected as variance reduction methods. The cell importance for both electrons and photons were set at one for all program cells, but 100 for tally

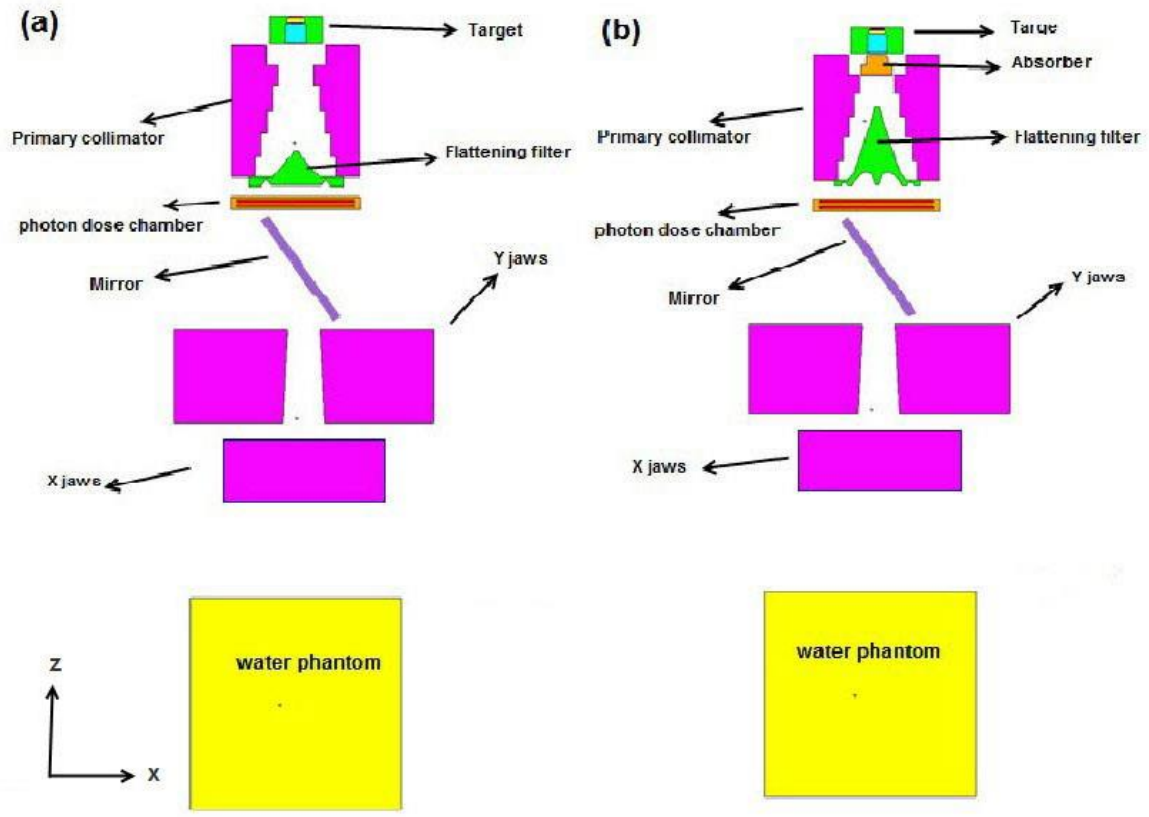

Figure 1: Schematic view of Siemens Primus plus (KD2) accelerator in photon mode (Y-Z view) for: 6 MV photon beam (a); and for 18 MV photon beam (b).

Table 1: The material components of the linac head for 6 MV and 18 MV photon beam energies of a Siemens Primus Plus

Element	Material
Jaws	Tungsten
Mirror	Silicon oxide (SiO_2)
Target	Gold
Absorber	Aluminium
Flattening filter	Stainless steel alloy (SST-303)
Primary collimator	Tungsten
Photon dose chamber	Aluminium oxide (Al_2O_3-alumina)

cells inside the phantom. A total of 2×10^9 particles were run in the simulation of accelerator head for 5×5 cm^2, 10×10 cm^2 and 20×20 cm^2 field sizes.

Moreover, the energy cut-off for electron and photon were set to be 500 keV and 10 keV, respectively. F6 tally was used for calculating the average energy in cells and *F8 tally for that of energy deposition. In the build-up region, *F8 tally value was divided by the mass of the tally cell to obtain the energy deposition per unit mass of the tally voxel. For F6 tally results, the maximum statistical type A uncertainty in MC calculations was 0.3%, while for *F8 tally was 0.8%. The mesh tally method was also used as a supportive measure, with several programs implemented.

For computing the percentage depth dose (PDD) in cells, we selected some cylinders with radius of 1 cm for different fields. The height of these cylinders ranged from 1 mm to 10 mm inside the phantom, perpendicular to the surface of the phantom. For better consequences, voxels with disparate sizes were used, for example in the build-up area; the cells were much smaller than the cells in the tail area of PDD curve.

Table 2: Flattening filter (FF) and primary collimator (PC) parameters for 6 MV photon beam

Layer	Number of layer	Number of cones	Material
1 PC	1	1	Tungsten
2 PC	2	1	Tungsten, air
3 PC	3	1	Tungsten, air
4 PC	4	1	Tungsten, air
5 PC	5	1	Tungsten, air
5 PC+ 1 FF	6	2	Stainless steel, tungsten, air
6 PC+1 FF	7	2	Stainless steel, tungsten, air
6 PC +2 FF	8	2	Stainless steel, tungsten, air
6 PC +3 FF	9	2	Stainless steel, tungsten, air
4 FF	10	1	Stainless steel, air
5 FF	11	1	Stainless steel, air
6 FF	12	1	Stainless steel, air

The radius of the cells in the phantom was selected to be one tenth of the field size, so that better results for PDD could be obtained [12]. The PDD value gives lone section of the information needed for a correct dose inside the phantom. For this reason, data related to the curve of dose profile were obtained. The beam profile is very significant in the credibility of Monte Carlo simulation because it renders information about the veracity of building of each component in the linear accelerator head. The main components, which have a main effect on the beam profile, are flattening filter and secondary collimators. Any variation on size or situation of one of these components will affect directly the shape of beam profile [5].

Therefore, dose profiles for 5 × 5 cm^2, 10 × 10 cm^2 and 20 × 20 cm^2 field sizes were obtained at different depths. Moreover, in order to calculate the dose profile inside the phantom, cells in different modes were selected; in the first case, cells were cylinders with radius of 2 mm and length of 1 mm in the direction of *X*-axis arrayed along *X*-axis at different depths in the phantom (*X*-axis is parallel to the phantom surface and Z-axis is perpendicular to the phantom surface). In these calculations, the maximum statistical type A uncertainty in MC calculations was 8%.

In the second mode, cells were cylinders with 1 mm radius and 2 mm length in the direction of *X*-axis arrayed along *X*-axis at different depths of the phantom for different field sizes; and the maximum statistical type A uncertainty in MC calculations was 7%. The third mode of the cells was sticking together and they were cylinders with 1 mm radius and 10 mm length in the direction of *Y*-axisto be arrayed along *X*-axis at different depths of the phantom for different field sizes; and the maximum statistical type A uncertainty in MC calculations was 6%. In the fourth mode of cells, they were not sticking together, were cylinders with 1 mm radius and 10 mm length in the direction of Y-axis, and were arrayed along *X*-axis for different field sizes, located at different depths of the phantom; and the maximum statistical type A uncertainty in MC calculations was 3%. The fourth mode produced better results with fewest discrepancies because it lacked gradient dose and overlapping (directions marked in Figure 1).

In order to evaluate the accuracy of dose calculations performed by MC modelling of a linear accelerator head, calculations with direct

Table 3: Flattening filter (FF), primary collimator (PC) and absorber (abs) parameters for 18 MV photon beam

Layer	Number of layer	Number of cones	Material
1 PC	1	0	Tungsten, air
1 PC+1 abs	2	0	Aluminium (Al), tungsten
1 PC+ 2 abs	3	0	Aluminium (Al), tungsten
1 PC+ 3 abs	4	0	Aluminium (Al), tungsten
1 PC+ 4 abs	5	0	Aluminium (Al), tungsten
2 PC	6	0	Air, tungsten
3 PC	7	0	Air, tungsten
3 PC + 0 FF	8	1	Stainless steel, tungsten, air
3 PC + 1 FF	9	1	Stainless steel, tungsten, air
3 PC + 2 FF	10	1	Stainless steel, tungsten, air
4 PC+ 2 FF	11	1	Stainless steel, tungsten, air
4 PC+ 3 FF	12	1	Stainless steel, tungsten, air
5 PC+ 3 FF	13	1	Stainless steel, tungsten, air
5 PC + 4 FF	14	1	Stainless steel, tungsten, air
6 PC + 4 FF	15	1	Stainless steel, tungsten, air
6 PC + 5 FF	16	1	Stainless steel, tungsten, air
6 PC + 6 FF	17	2	Stainless steel, tungsten, air
6 PC + 7 FF	18	3	Stainless steel, tungsten, air
6 PC + 8 FF	19	3	Stainless steel, tungsten, air
6 PC + 9 FF	20	3	Stainless steel, tungsten, air
6 PC+10 FF	21	3	Stainless steel, tungsten, air
6 PC+11 FF	22	3	Stainless steel, tungsten, air
6 PC+12 FF	23	3	Stainless steel, tungsten, air
6 PC+13 FF	24	3	Stainless steel, tungsten, air
14 FF	25	2	Stainless steel, air
15 FF	26	2	Stainless steel, air
16 FF	27	2	Stainless steel, air
17 FF	28	2	Stainless steel, air

measurement are needed. For this purpose, experimental measurement of data for PDD and dose profile was performed in a cubic phantom using PTW Semiflex 31010 ionization chamber. Uncertainty is the parameter that describes the distribution of measured values of a quantity. To reduce MC uncertainties for each program with 2 billion particles, twenty programs (with different random seed numbers for each mode) were run using DBCN card in MCNP.

These repeated programs reduce the total uncertainty, and the total uncertainty is calculated as follows:

$$\text{Total uncertainty} = \sqrt{\left(\frac{n_1}{N}\right)^2 \sigma_1^2 + \left(\frac{n_2}{N}\right)^2 \sigma_2^2 + \ldots + \left(\frac{n_m}{N}\right)^2 \sigma_m^2} \quad (1)$$

Where n_1, n_2, etc. are the number of particles in each program and m is the total number of programs. Furthermore, N is the total number of particles in all programs. σ_1, σ_2, etc. are uncertainties in programs No. 1, 2, etc.

The percentage depth dose (PDD) was normalized against the maximum dose and plotted for 5 × 5 cm², 10 × 10 cm² and 20 × 20 cm² field sizes for 6 MV and 18 MV photon beams as shown in Figure 2 and Figure 3. Dose profile was normalized to the midpoint and plotted for 5 × 5 cm², 10 × 10 cm² and 20 × 20 cm² field size at dmax, 5 cm and 10 cm for 6 MV and 18 MV beams as is shown in Figures 4 and 5. The discrepancy between the results of calculations and measurements can be expressed according to:

$$\Delta = 100 \times \left(\frac{V_{MC} - V_{\exp}}{V_{\exp}}\right) \qquad (2)$$

Where V_{MC} is the value calculated by *MC* simulation and V_{exp} is the experimental value. Gamma function was also used to compare *MC* with the experimental data.

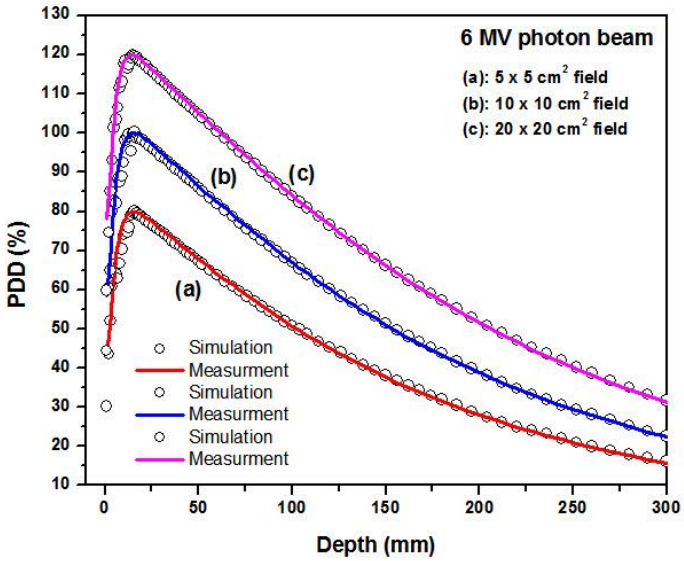

Figure 2: PDD value from simulation and measurement results versus depth for 6 MV photon beam. (a): for 5 × 5 cm² field; (b): for 10 × 10 cm² field; (c): for 20 × 20 cm² field. To avoid overlapping of the curves, the data were multiplied by factors (0.8, 1 and 1.2, respectively).

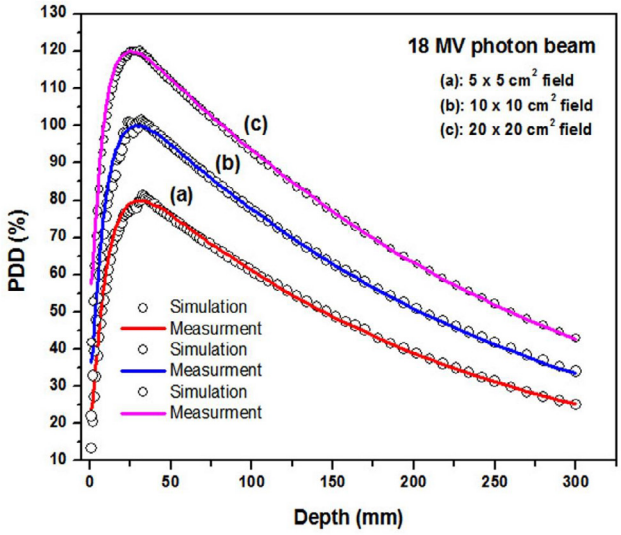

Figure 3: PDD value from simulation and measurement results versus depth for 18 MV photon beam. (a): for 5 × 5 cm² field; (b): for 10 × 10 cm² field; (c): for 20 × 20 cm² field. To avoid overlapping of the curves, the data were multiplied by factors (0.8, 1 and 1.2, respectively).

PDD and Dose Profile Comparisons using Gamma Function

The comparisons of PDD and dose profile values acquired by MC simulations and measurements were done by the calculation of gamma function. This function is a helpful tool for analogy of two dose distributions: one as the computed dose distribution that should be evaluated. Gamma function combines two criteria, which have been previously used in comparisons of two dose distributions: the percentage dose difference (DD) in terms of percentage, and distance to agreement (DTA) in terms of mm. When only dose difference is used, it is sensitive in high-dose gradient regions. However, DTA criterion is sensitive in low-dose gradient regions; therefore, it is useful to combine both criteria for the calcu-

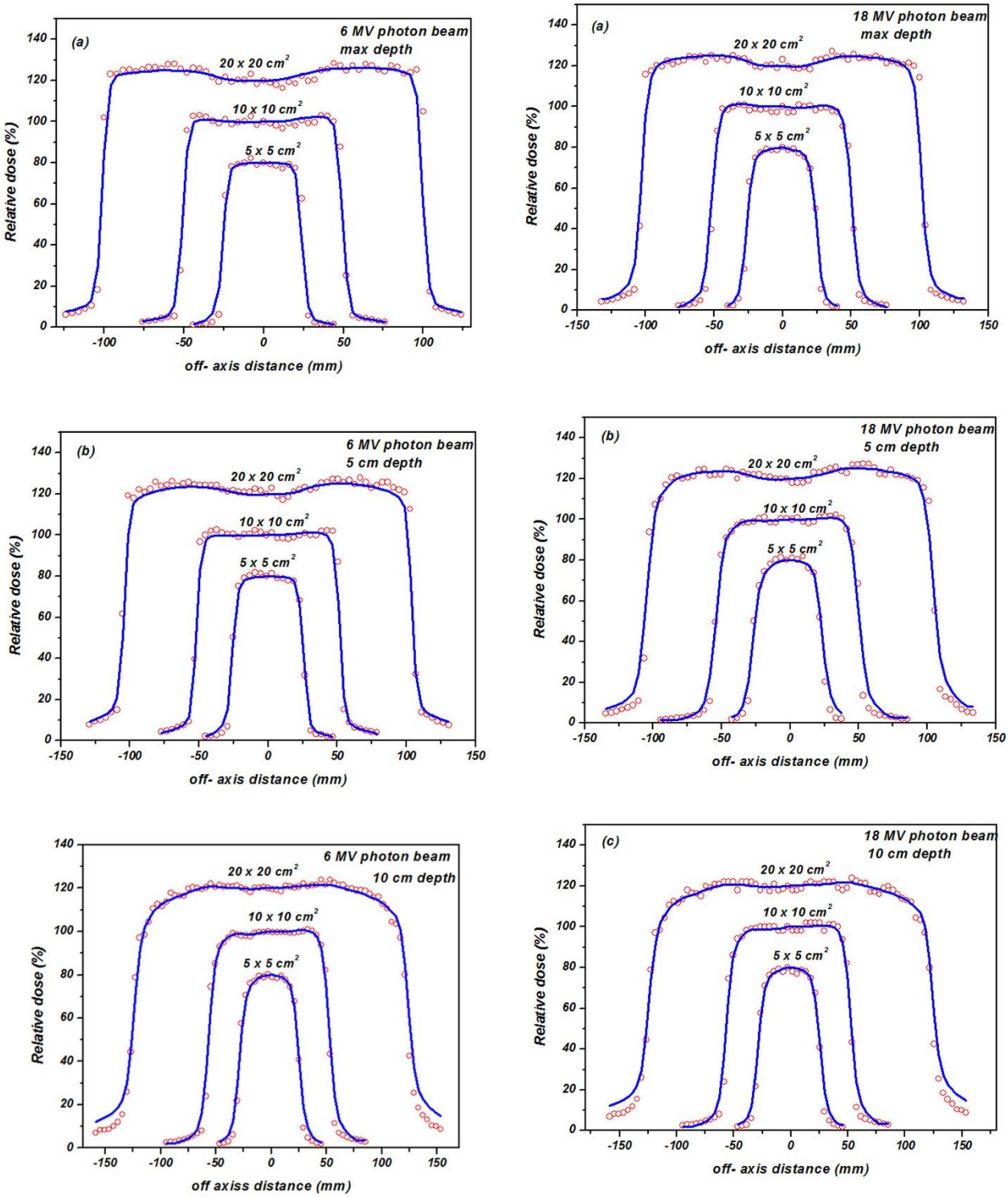

Figure 4: Beam dose profile from calculation and measurement for 6 MV photon beam. (a): for maximum depth; (b): for 5 cm depth; (c): for 10 cm depth. To avoid overlapping of the curves, the data were multiplied by factors (0.8, 1 and 1.2, respectively).

Figure 5: Beam dose profile from calculation and measurement for 18 MV photon beam. (a): for maximum depth; (b): for 5 cm depth; (c): for 10 cm depth. To avoid overlapping of the curves, the data were multiplied by factors (0.8, 1 and 1.2, respecively).

lation of a dual gamma function. Gamma index (function) has two edgy values: 0 and 1. Gamma functions between zero and unity are considered as pass or agreement, while gamma values higher than unity are considered as fail or disagreement. The followings are its mathematical composition related to gamma function calculation:

$$\gamma(\mathrm{r}_r) = \min\{\Gamma(\mathrm{r}_r, \mathrm{r}_e)\} \forall \{\mathrm{r}_e\} \quad (3)$$

$$\Gamma(\mathrm{r}_r, \mathrm{r}_e) = \sqrt{\frac{r^2(\mathrm{r}_r, \mathrm{r}_e)}{\Delta d^2_{\max}} + \frac{\delta^2(\mathrm{r}_r, \mathrm{r}_e)}{\Delta D^2_{\max}}} \quad (4)$$

$$r(\mathrm{r}_r, \mathrm{r}_e) = |\mathrm{r}_e - \mathrm{r}_r| \, \delta(\mathrm{r}_r, \mathrm{r}_e) = D_e(\mathrm{r}_e) - D_r(\mathrm{r}_r) \quad (5)$$

$$\Gamma(r_r, r_e) = 1 \quad (6)$$

$\gamma(\mathrm{r}_r)$ is acceptable for $0 \le \gamma(\mathrm{r}_r) \le 1$ and is not acceptable for $\gamma(\mathrm{r}_r) > 1$. The dose-difference criterion is $\Delta D_{\max}$, and the DTA criterion is $\Delta d_{\max}$. The passing criteria shown for the examples are $\Delta D_{\max}$ =3% and $\Delta d_{\max}$ = 3 mm based on our internal clinical standards for photon beams. δ represents the difference between the measured and calculated doses [12]. In order to calculate gamma function, PDD values from MC simulation were incorporated in a text file. PDD values acquired by measurement were also incorporated in another text file. The two text files then were processed by gamma function calculation software as input files to calculate gamma indices versus depth (mm) for the two relative dose distributions. In the present study, the gamma function software provided by DOSIsoft Company was used to calculate one-dimensional gamma indices. The software is called gamma_index.exe and works in Gnuplot software (version 4.4 patch level 3, Geeknet Inc. Fairfax, VA, USA) environment. DD and DTA criteria were set, respectively, as 3% and 3 mm in gamma index calculations by gamma-index software [13-15].

Results and Discussion

The simulated PDD values for 5 × 5 cm^2, 10 × 10 cm^2 and 20 × 20 cm^2 field sizes were compared with those measured in water for 6 MV and 18 MV as shown in Figure 2 and 3, respectively. It should be mentioned that the PDD for 5 × 5 cm^2 and 20 × 20 cm^2 were multiplied by factors of 0.8 and 1.2, respectively, in order to be distinguished from the PDD for the 10 × 10 cm^2 field.

For PDD of 6 MV and 18 MV energies, the measured and simulated data for the depths outside $d_{\max}$ had a good settlement, less than 2% difference, so that at 6 MV, the difference between the dose calculated by MC and the results from in-phantom measurement was less than 1%, except in the build-up area. The same is true for 18 MV beam with a difference of less than 2%, except for the build-up area. In the build-up region, the difference was 4% for the 6 MV photon beam and 8% for the 18 MV photon beam. To have more accurate results, vowels with various sizes were used, for example, in the build up region, vowels were much smaller than those in the distal part of PDD curves were. The radius of the cells in phantom was selected to be one tenth of the field size, so that more accurate results for PDD could be obtained than expected [13].

Figures 4 and 5 present dose profiles for 6 MV and 18 MV energies at different depths, specified by measurement and MC simulation for 5 × 5 cm^2, 10 × 10 cm^2 and 20 × 20 cm^2 field sizes. The dose profiles show a nearly good agreement with the measurement for all depths. Additionally, the configuration of the simulated dose profile matches well the measurement at the central area of dose profile. Moreover, in order to calculate the dose profile inside the phantom, cells in different modes were selected. In the first case, cells were selected as cylinders with radius of 2 mm and length of 1 mm in the direction of *X*-axis arrayed along *X*-axis at different depths in the phantom (*X*-axis is parallel to the phantom surface and Z-axis is perpendicular to the

phantom surface). In the second mode, cells were cylinders with 1 mm radius and 2 mm length in the direction of *X*-axis arrayed along *X*-axis at different depths of the phantom for different field sizes.

The third mode, cells were sticking together and they were cylinders with 1 mm radius and 10 mm length in the direction of *Y*-axis that were arrayed along X- axis at different depths of the phantom for different field sizes. The fourth mode, cells were not sticking together and the cylinders with 1 mm radius and 10 mm length in the direction of Y-axis, which were arrayed along *X*-axis for different field sizes, located at different depths of the phantom. The fourth mode produced better results with fewest discrepancies because it lacked gradient dose and overlapping. In a practical case, a dosimeter used for the calculation of dose profile is a cylinder perpendicular to *X*-axis, in the direction of Y-axis. For this reason, the fourth mode was considered for dose profile cells, and this method resulted in a good agreement between measurement and the Monte Carlo calculations.

The settlement in the penumbral area was better for 6 MV beam compared with 18 MV beam. The simulated PDD for 6 MV and 18 MV photon beam for 5 × 5 cm^2, 10 × 10 cm^2 and 20 × 20 cm^2 field sizes were compared with measurement values by gamma function as shown in Figures 6 and 7, respectively. The dose profile data for 5 × 5 cm^2, 10 × 10 cm^2 and 20 × 20 cm^2 field sizes were compared with measurement values by gamma function as shown in Figures 8 and 9.

For PDD and dose profile data, the agreement was acquired between two sets of data for both energies for all field sizes. For example, dose profile more than 90% of the points of the simulations had gamma values less than unity and for PDD nearly all data of the points of the simulations had gamma values less than unity. In this situation, the difference between MC and measurement of PDD values were within 1% in the tail region of PDD curve. Gamma function assessment shows that there was generally a good settlement between the measured and calculated PDD data. In gamma function calculations, the dose difference and the distance to agreement criteria were 3% and 3 mm, respectively. A gamma value of equal to or less than 1.00 means that these two dose data sets are in agreement [14]. The measured and calculated amounts of self-relative dose at depths of 4 and 5 cm, and the ratio of dose for 6 MV and 18 MV photon beams for 10 × 10 cm^2 field sizes at depths of 20 cm and 10 cm (D_{20}/D_{10}) are compared in Tables 4 and 5. The discrepancy between simulated and measured data in these depths is very scant, and the ratio of D_{20}/D_{10} is negligible. DD and DTA indices used in calculation gamma functions were respectively set as 3% and 3 mm.

Table 4: Calculated and measured data of PDD (%) for 6 MV photon beam for 10 × 10 cm^2 field at depths of 4 and 5 cm and D_{20}/D_{10}, which is the ratio of depth doses on the central axis, at 20 cm and 10 cm depths, respectively.

	4 cm	5 cm	D_{20}/D_{10}
Simulation	90.1±1.7	86.6±1.1	0.59±0.05
Measurement	90.9±1.2	86.7±1.6	0.58±0.02

Table 5: Calculated and measured data of PDD (%) for 18 MV photon beam for 10 × 10 cm^2 field at depths of 4 and 5 cm (%) and D_{20}/D_{10}, which is the ratio of depth doses on the central axis, at 20 cm and 10 cm depths, respectively.

	4 cm	5 cm	D_{20}/D_{10}
Simulation	98.3±1.8	94.6±1.8	0.66±0.01
Measurement	98.4±1.9	94.7±1.2	0.65±0.04

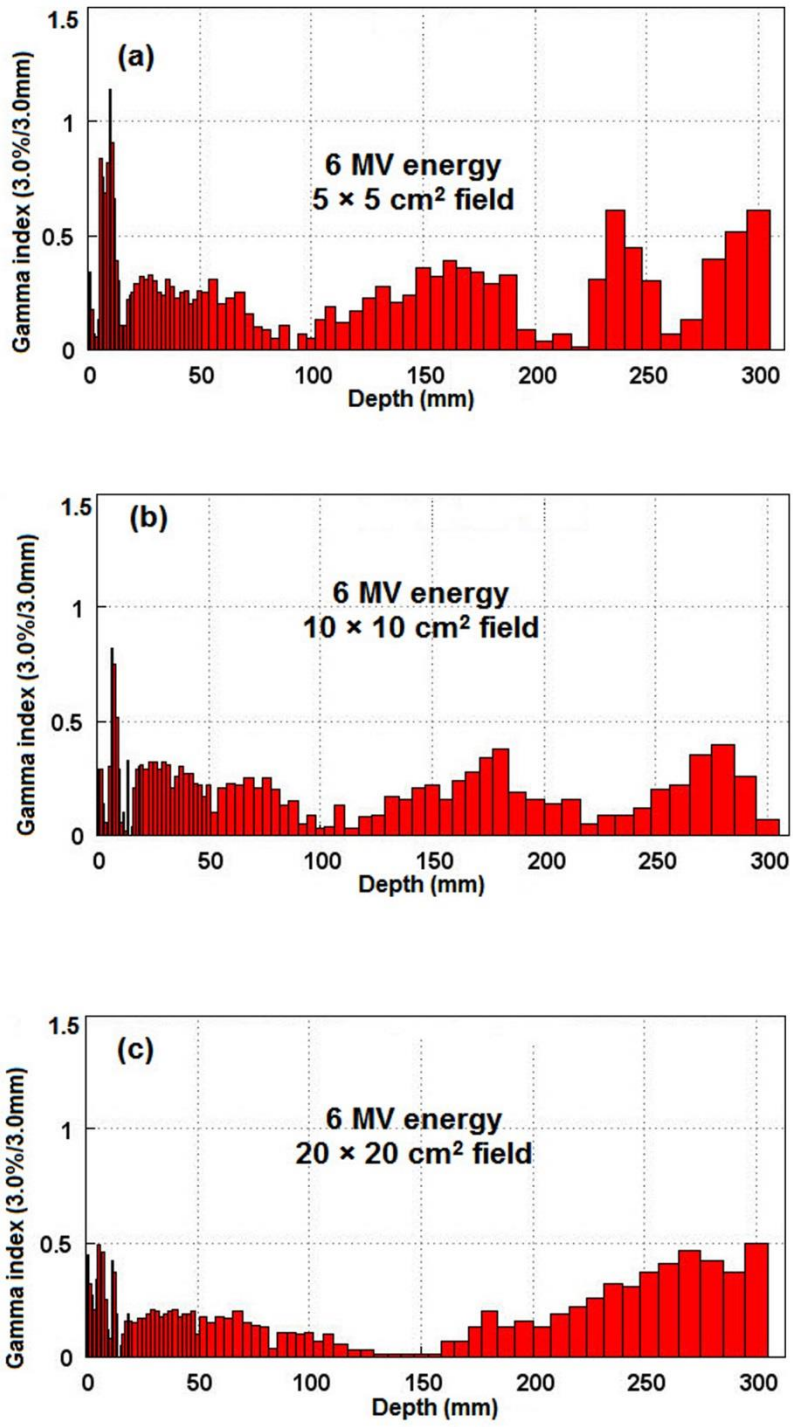

Figure 6: Gamma index values versus depth (mm) in phantom for various fields for comparison of PDD values. Parts (a), (b) and (c) in the figure are related to 6 MV photon energy, for 5 × 5 cm^2, 10 × 10 cm^2, 20 × 20 cm^2 fields, respectively.

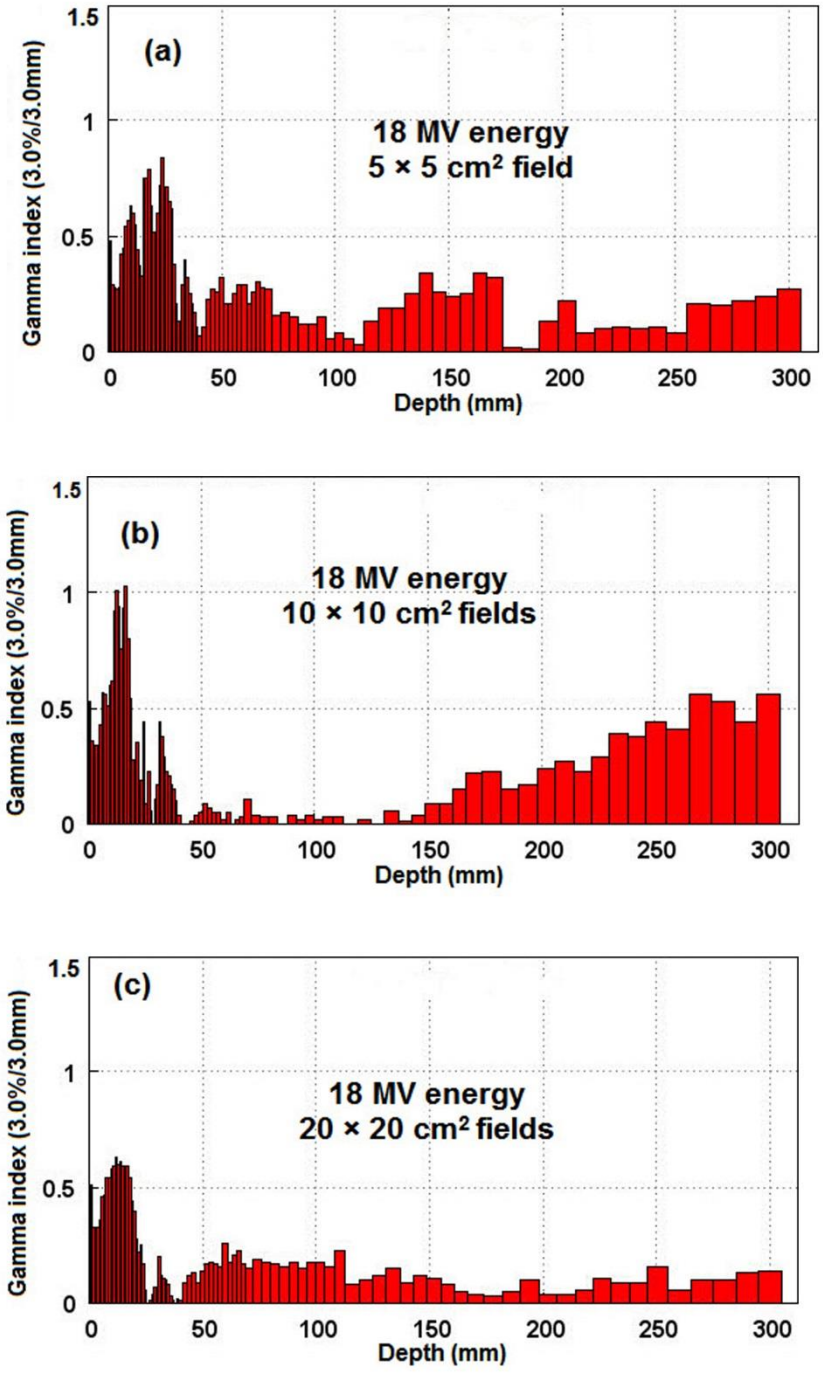

Figure 7: Gamma index values versus depth (mm) in phantom for various fields for comparison of PDD values. Parts (a), (b) and (c) in the figure are related to 18 MV photon energy, for 5 × 5 cm^2, 10 × 10 cm^2 and 20 × 20 cm^2 fields, respectively.

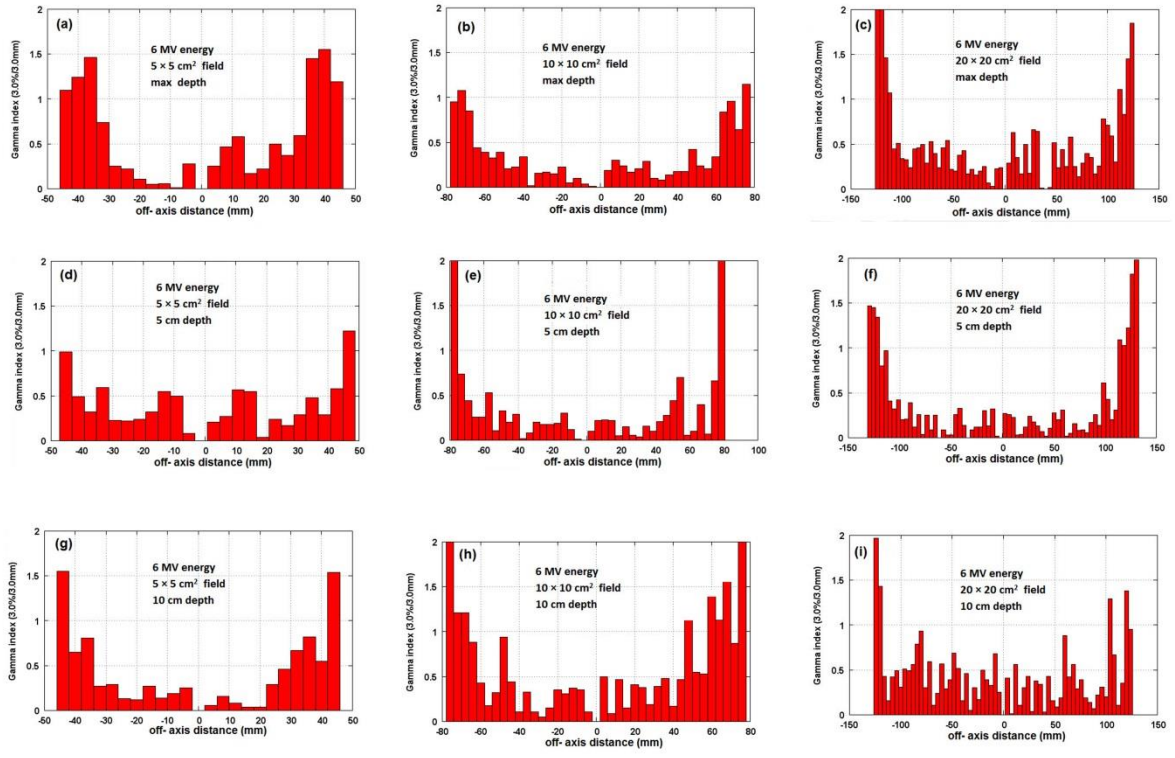

Figure 8: Gamma index values versus off-axis distance in phantom (mm) for various fields. Parts (a), (b) and (c) are related to 6 MV photon beam at dmax for 5 × 5 cm², 10 × 10 cm² and 20 × 20 cm² fields, respectively. Parts (d), (e) and (f) in the figure are related to 6 MV photon beam at 5 cm depth for 5 × 5 cm², 10 × 10 cm² and 20 × 20 cm² fields. Similarly parts (g), (h) and (i) are related to 6 MV photon beam, at 10 cm depth for 5 × 5 cm², 10 × 10 cm² and 20 × 20 cm² fields.

Conclusion

In this study, the simulation of Siemens Primus Plus linear accelerator was performed for beam energies of 6 and 18 MV, values of PDD and dose profiles were obtained. The optimized energy of electron spectrum was selected within ± 0.2 MeV energy range self-relative to the manufacturer-provided energy spectrum. The selection of the optimized energy was firmly fixed on the settlement of build-up depth determined from empirical measurement with MC simulations. For PDD, the difference between calculated and measurement values for 6MV and 18 MV energies was within 2%.

For PDD of 6 MV and 18 MV energies, the measured and simulated data for the depths outside dmax had a good settlement, less than 2% difference, so that at 6 MV, the difference between the dose calculated by MC and the results from in-phantom measurement was less than 1%, except in the build-up area. The same is true for 18 MV beam with a difference of less than 2%, except for the build-up area. In the build-up region, the difference was 4% for 6 MV photon beam and 8% for 18 MV photon beam.

In dose profile results, the agreement between MC and measured values were not very significant, particularly in the boundary points, this point is observed in some studies [16]. Since the comparisons proved this modeling credible, for 18 MV accelerators photon energy, one can study dose repartition in different geometries and assessment the neutron dose received by the patient. Simulation programs can be used for photon modes of Siemens Primus Plus linac in situation which is

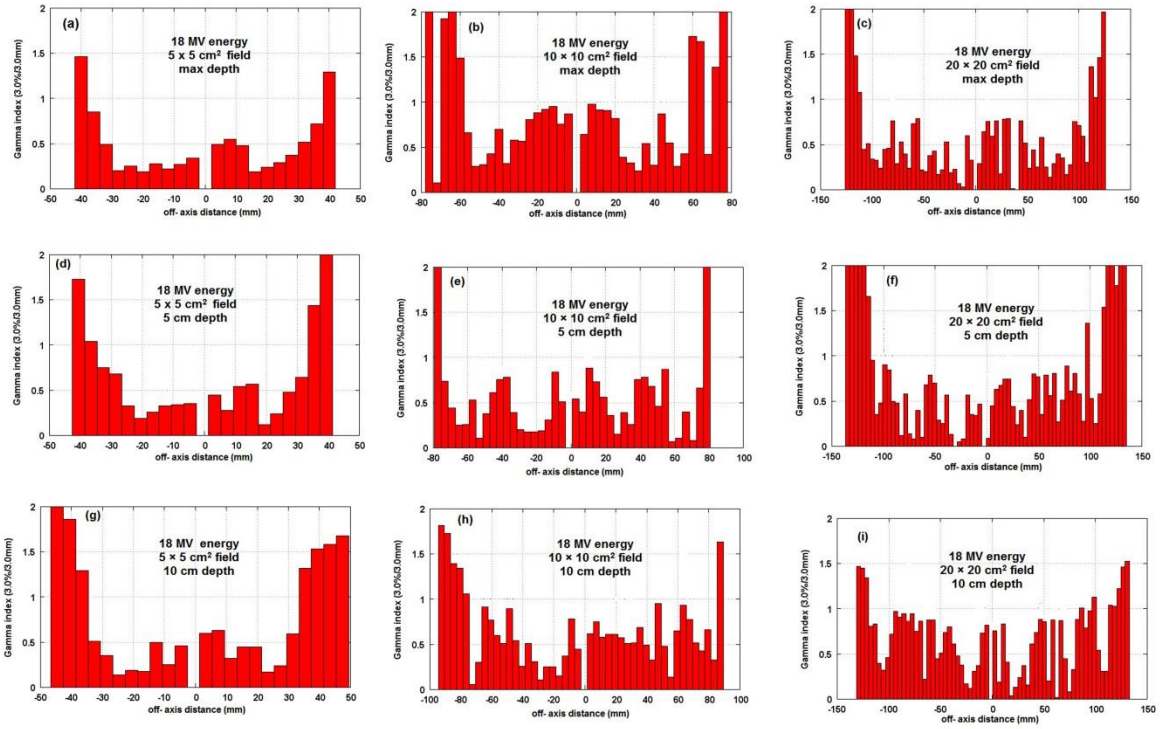

Figure 9: Gamma index values versus off-axis distance in phantom (mm) for various fields. Parts (a), (b) and (c) are related to 18 MV photon beam at dmax for 5 × 5 cm^2, 10 × 10 cm^2 and 20 × 20 cm^2 field, respectively, Parts (d), (e) and (f) in the figure are related to 18 MV photon beam at 5 cm depth for 5 × 5 cm^2, 10 × 10 cm^2, 20 × 20 cm^2 field. Similarly parts (g), (h) and (i) are related to 18 MV photon beam, at 10 cm depth for 5 × 5 cm^2, 10 × 10 cm^2, and 20 × 20 cm^2 field.

not pragmatic to perform in-phantom or in-patient measurement.

Acknowledgment

The authors appreciate Payame Noor University of Mashhad for financial support of this project.

Conflict of Interest

There is not any relationship that might lead to a conflict of interest. Payame Noor University of Mashhad financially supported the work and this is stated in the acknowledgment section of the article.

References

1. Vega-Carrillo HR, Martinez-Ovalle SA, Lallena AM, Mercado GA, Benites-Rengifo JL. Neutron and photon spectra in LINACs. *Appl Radiat Isot*. 2012;**71**:75-80. doi.org/10.1016/j.apradiso.2012.03.034. PubMed PMID: 22494894.
2. Becker J. Simulation of neutron production at a medical linear accelerator: Diploma thesis, Department of Physics, University of Hamburg performed at the University Medical Center Hamburg-Eppendorf, Department of Radiotherapy and Radio-Oncology, Medical Physics; 2007.
3. Ma CM, Jiang SB. Monte Carlo modelling of electron beams from medical accelerators. *Phys Med Biol*. 1999;**44**:R157-89. doi.org/10.1088/0031-9155/44/12/201. PubMed PMID: 10616140.
4. Bahreyni Toosi M, Momen Nezhad M, Saberi H, Bahreyni Toosi M, Hashemian A, Salek R, et al. A Monte Carlo simulation of photon beam generated by a linear accelerator. *Iranian Journal of Medical Physics*. 2005;**2**:3-12.
5. Aljamal M, Zakaria A. Monte Carlo Modeling of a Siemens Primus 6 MV Photon Beam Linear Accelerator. *Australian Journal of Basic and Applied Sciences*. 2013;**7**:340-6.
6. Grevillot L, Frisson T, Maneval D, Zahra N, Badel JN, Sarrut D. Simulation of a 6 MV Elekta Precise

Linac photon beam using GATE/GEANT4. *Phys Med Biol*. 2011;**56**:903-18. doi.org/10.1088/0031-9155/56/4/002. PubMed PMID: 21248389.

7. Sardari D, Maleki R, Samavat H, Esmaeeli A. Measurement of depth-dose of linear accelerator and simulation by use of Geant4 computer code. *Rep Pract Oncol Radiother*. 2010;**15**:64-8. doi.org/10.1016/j.rpor.2010.03.001. PubMed PMID: 24376926. PubMed PMCID: 3863189.
8. Becker J, Brunckhorst E, Schmidt R. Photoneutron production of a Siemens Primus linear accelerator studied by Monte Carlo methods and a paired magnesium and boron coated magnesium ionization chamber system. *Phys Med Biol*. 2007;**52**:6375-87. doi.org/10.1088/0031-9155/52/21/002. PubMed PMID: 17951849.
9. Mohammadi N, Miri Hakimabad SH, Rafat Motavali L, Akbari F, Abdollahi S. Neutron spectrometry and determination of neutron contamination around the 15 MV Siemens Primus LINAC. *Journal of Radioanalytical and Nuclear Chemistry*. 2015;304. doi.org/10.1007/s10967-015-3944-5.
10. Chetty IJ, Curran B, Cygler JE, DeMarco JJ, Ezzell G, Faddegon BA, et al. Report of the AAPM Task Group No. 105: Issues associated with clinical implementation of Monte Carlo-based photon and electron external beam treatment planning. *Med Phys*. 2007;**34**:4818-53. doi.org/10.1118/1.2795842. PubMed PMID: 18196810.
11. Mckinney G, Durkee J, Hendricks J, James M, Pelowitz D. MCNPX USERS MANUAL, Version 2.7. 0. LA-CP-11-00438,"LANL, Los Alamos, 2011.
12. Allahverdi M, Zabihzadeh M, Ay M, Mahdavi S, Shahriari M, Mesbahi A, et al. Monte Carlo estimation of electron contamination in a 18 MV clinical photon beam. *Iranian Journal of Radiation Research*. 2011;**9**:15.
13. Low DA, Harms WB, Mutic S, Purdy JA. A technique for the quantitative evaluation of dose distributions. *Med Phys*. 1998;**25**:656-61. doi.org/10.1118/1.598248. PubMed PMID: 9608475.
14. Toossi MTB, Ghorbani M, Akbari F, Sabet LS, Mehrpouyan M. Monte Carlo simulation of electron modes of a Siemens Primus linac (8, 12 and 14 MeV). *Journal of Radiotherapy in Practice*. 2013;**12**:352-9. doi.org/10.1017/S1460396912000593.
15. Depuydt T, Van Esch A, Huyskens DP. A quantitative evaluation of IMRT dose distributions: refinement and clinical assessment of the gamma evaluation. *Radiother Oncol*. 2002;**62**:309-19. doi.org/10.1016/S0167-8140(01)00497-2. PubMed PMID: 12175562.
16. Tzedakis A, Damilakis JE, Mazonakis M, Stratakis J, Varveris H, Gourtsoyiannis N. Influence of initial electron beam parameters on Monte Carlo calculated absorbed dose distributions for radiotherapy photon beams. *Med Phys*. 2004;**31**:907-13. doi.org/10.1118/1.1668551. PubMed PMID: 15125009.